View metadata, citation and similar papers at core.ac.uk
brought to you by CORE
provided by University of Huddersfield Repository

Efficient Implementation of Envelope Analysis on Resources Limited Wireless Sensor Nodes for Accurate Bearing Fault Diagnosis

G Feng [a], H Zhao [b], F Gu [a], P Needham [a] and A D Ball [a]

[a] University of Huddersfield, Queensgate, Huddersfield, HD1 3DH, United Kingdom

[b] Shandong University of Science and Technology, Shandong, 266590, China

Abstract:

With the fast development of electronics and wireless communication technologies in recent years, intelligent wireless sensor nodes are becoming increasingly popular in the online machinery condition monitoring systems. They bring a number of benefits, such as reduced investment on the installation and maintenance of expensive communication cables, ease of deployment and upgrading. For the condition monitoring of dynamic signals, distributed computation on wireless sensor nodes is getting popular with wireless sensor nodes becoming more computation powerful and power efficient. As a widely recognised algorithm for bearing fault diagnosis, envelope analysis has been previously proved suitable for being embedded on the wireless sensor nodes to effectively extract fault features from common machinery components such as bearings and gears. As a continuation, this paper studies into several envelope detection methods, including Hilbert transform, spectral correlation, band-pass squared rectifier and short-time RMS. Regarding to the fact that only low frequency components in the bearing envelope is of interest, spectral correlation can be simplified for fast calculation and short-time RMS method can be considered as a simplified band-pass squared rectifier, in which partial aliasing is allowed. Thereafter, spectral correlation and short-time RMS are employed to speed up the calculation of envelope analysis on a wireless sensor node, which thereafter provides the potential to reduce power consumption of wireless sensor nodes. The computation speed comparison shows that the spectral correlation method and short-time RMS can speed up the computation speed by more than two times and five times in comparison with the Hilbert transform method. The simulation study shows that spectral correlation and short-time RMS based methods achieves similar level of accuracy as Hilbert transform. Furthermore, the experimental study shows that spectral correlation and short-time RMS based methods can well reveal the simulated three types of bearing faults while with the computation speed significantly improved.

Keywords: Envelope analysis, Hilbert transform, Spectral correlation, Short-time RMS, Wireless sensor node, Fault diagnosis.

1 Introduction

With the fast development of electronics and wireless communication technologies in recent years, intelligent wireless sensor nodes are becoming increasingly popular in the online condition monitoring (CM) systems [1], [2]. They bring numerous benefits, such as reduced costs of the installation and maintenance of expensive communication cables, ease of deployment and upgrading.

In a vast number of scenarios, wireless sensor nodes are powered by batteries, which means they have limited energy and need to be changed/replaced regularly. To reduce such maintenance operations, wireless sensor nodes are usually designed with restricted computation capability and limited memory to keep their power consumption to a minimum level and thus prolong their lifespan. In recent years, different energy harvesting techniques are emerging to provide power for the sensor nodes by absorbing energy from their ambient environment, like wasted heat [3] or mechanical

vibrations [4] from machines. By utilising such energy resources, it is expected to significantly prolong the lifespan of these wireless sensor nodes. In the meantime, energy harvested from such resources are usually limited, for example, the energy harvested from temperature gradient is only 10 μW/cm^3 and that from vibrations is about 200 μW/cm^3 (for consultancy, the energy from direct sun is 15000 μW/cm^3) [5]. Therefore, it is still crucial to utilise the limited power wisely.

To minimise power consumption, the popular wireless communication protocols utilised in the wireless sensor networks typically have a low transmission data rate. For instance, the maximum data rate of Zigbee and WirelesHart is 250 kbps and that of Bluetooth Low Energy (BLE) is restricted to 1 Mbps. In practice, their data throughput can be even lower than this due to packet overhead, multi-hop and transmission faults [6]. Such a data throughput is sufficient for static type signals, like temperature, pressure, etc. However, they become incompetent for dynamic type signals, like vibration, acoustics and motor current. In practice, these dynamic signals are widely employed for the condition monitoring of rotating machines and are usually more helpful for analysing dynamic behaviour and diagnosing faults in such machines [7].

For processing such dynamic signals, distributed computation scheme can be more suitable than the common centralised computation scheme. In distributed computation scheme, the large raw data set is pre-processed on the wireless sensor nodes and only the resultant data set containing sufficient diagnosis information is transmitted over the bandwidth limited wireless network. By utilising such a scheme, not only the limited bandwidth can be well utilised but also it has the potential to save the valuable power energies of sensor nodes [8].

With the advancement in electronics technology, the sensor nodes are becoming more powerful, with more computation capability but less power consumption. This has reduced the challenges in embedding intelligent signal processing algorithms on resource limited wireless sensor nodes. For this reason, distributed computation is becoming increasingly popular in wireless CM in recent years. In [9], Sreenuch et al. proposed an approach for distributed CM systems that offers a reusable software architecture for a number of applications. Yin and Zhong [10] monitored rotating auxiliaries at power plants based on a distributed wireless vibration based CM system, in which they employ a data-level fusion for comparing the similarity of adjacent data and a task-level fusion for providing the strategy of sending data and the way to judge nodes' survival. Hou et al. [1] proposed a scheme for induction motor condition monitoring and fault diagnosis based on motor stator current and the vibrational signatures. In this system, feature extraction and classification by the neural network classifier are implemented on the node and decision level fusion is executed at the centre.

As a widely accepted algorithm for the fault diagnosis of bearings and gears, envelope analysis has been proved to be an effective method for extracting bearing fault features on resources limited wireless sensor nodes. The authors implemented envelope analysis on a wireless sensor node to extract bearing fault features and the results showed that envelope analysis can produce a small resultant data set while retaining key bearing fault diagnosis information [11]. On this basis, a down-sampling and cascading scheme was proposed to increase the envelope spectrum resolution so as to

improve the fault diagnosis accuracy [12]. Furthermore, the fast kurtogram method was brought into the wireless CM network to adjust the band-pass filter adaptively [13], which has improved the robustness of the envelope analysis. Although the previous implementations have been optimised to well utilise the limited computation and memory resources, the calculation of envelope analysis, especially the envelope detection part, is still rather time consuming, requiring the embedded processor to run almost at full speed to finish the frame calculations in time.

This paper studies into the envelope analysis and tries to find more efficient implementations suitable for resources limited wireless sensor nodes. The structure of this paper is organised as follows. Section 2 discusses the theoretical background for the envelope detection methods, including envelope analysis, spectral correlation, band-pass squared rectifier and short-time RMS. Then, spectral correlation and short-time RMS are selected for implementation in Section 3. A simulation study is conducted in Section 4 to prove the effectiveness of the implemented methods for extracting bearing fault features and an experimental study is performed in Section 5 to compare the processing results of Hilbert transform, spectral correlation and short-time RMS. Finally, the conclusion is drawn in Section 6.

2 Theoretical background

2.1 Envelope analysis and its implementation

Envelope analysis calculates the frequency spectrum of the envelope of a signal. It is suitable for extracting fault features from impulsive and modulating type signals, which can be found in many key machinery components, such as bearings [14], [15], gears [16], turbines [17] and valves [18]. This type of signal is characterised by the presence of a periodic repetition of sharp peaks modulated by high-frequency resonance components [19]. Especially for rolling bearing diagnostics, envelope analysis has been recognised as the benchmark method over many years of development [20], [21].

As presented in Figure 1, the envelope analysis mainly includes three steps: band-pass filtration, envelope detection and power spectrum calculation. The band-pass filter is employed to enhance the signal to noise ratio (SNR) by rejecting low-frequency high-amplitude signals caused by imbalance or misalignment and eliminating random noises outside the pass-band [15]. The envelope detection extracts the modulating fault signal and transfers the high-frequency problem to a low-frequency one. The power spectrum step shows the frequency components in the detected envelope, namely envelope spectrum. By observing the envelope spectrum, the existence of localised bearing faults can be easily verified.

Figure 1 Procedures of envelope analysis

From the previous implementations, it is found the envelope detection is the most time consuming part in the calculation of envelope analysis. Normally, envelope analysis is performed by the Hilbert transform (HT) based method due to that it is more precise and is not sensitive to the carrier [22]. Supposing the HT of a real valued modulating signal $x(t)$ is $\tilde{x}(t)$, they can compose a complex signal $x_a(t)$ as presented in (1), such a signal is usually named as analytic or quadrature signal [22].

$$x_a(t) = x(t) + j\tilde{x}(t) \tag{1}$$

By calculating the amplitude of an analytic signal, the envelope of $x(t)$ can be obtained. The Fourier transform of the analytic signal $x_a(t)$ can be expressed as:

$$\begin{aligned} X_a(f) &= \begin{cases} 2X(f), & f > 0, \\ X(f), & f = 0, \\ 0, & f < 0 \end{cases} \\ &= 2u(f)X(f) \end{aligned} \tag{2}$$

where $X(f)$ is the Fourier transform of $x(t)$ and $u(f)$ is the step function.

A straight forward implementation of HT is the frequency domain method, as presented in Figure 2. In this method, an HT window is forced to apply on the spectrum $X(f)$ to obtain $X_a(f)$, which is then used to calculate the analytic signal $x_a(t)$. It can be observed this implementation includes two forward fast Fourier transform (FFT) and one inverse FFT (IFFT), which are the most time consuming part. This is the approach that the authors have employed in the previous studies [11]–[13]. Note that the band-pass filer is implemented in the frequency domain in Figure 2 to speed up the computation while it was previously implemented by a finite impulse response (FIR) filter in the time domain.

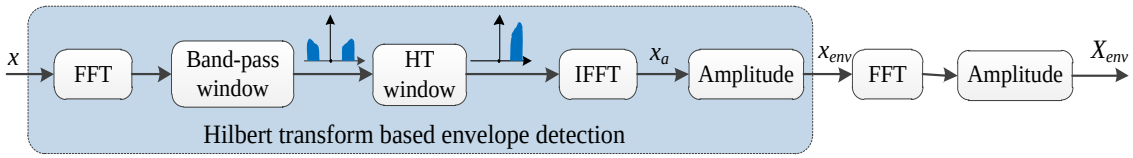

Figure 2 Schematic of frequency domain HT based envelope analysis

2.2 Spectral correlation

In Figure 2, the analytic signal x_a is obtained after the IFFT operation. By calculating the amplitude of the analytic signal x_a, the envelope of the input signal x can be obtained. Here, the amplitude is computed by the square root of the product of x_a with its conjugate x_a^* in the time domain. In the frequency domain, as shown in Figure 3, the product between x_a and x_a^* is equivalent to the convolution of X_a and G_a according to convolution theorem, where X_a and G_a are the FFT of x_a and x_a^*, respectively; $\bullet$ is the inner product operator and $\circledast$ is convolution operator. The result of convolution between X_a and G_a produces X_{envs}, which is the FFT of squared envelope x_{env}^2. In [14], Ho and Randall show that analysing the squared envelope can also verify the existence of localised bearing fault.

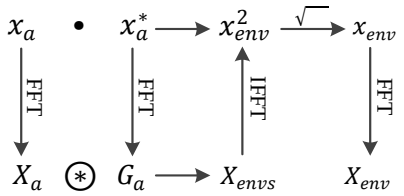

Figure 3 The amplitude calculation of analytic signal x_a in time domain and frequency domain

For X_a and G_a, they only contain either the positive or negative frequency components. According to the definition of $X_a(f)$ in Eq. (2), the Fourier transform of $x_a^*(f)$ can be derived as:

$$G_a(f) = 2u(-f)X^*(f) = X_a^*(-f) \tag{3}$$

This shows that the Fourier transform $G_a(f)$ of $x_a^*(t)$ can be obtained directly from the spectrum of $X(f)$. Thus, the convolution between $G_a[f]$ and $X_a[f]$ become:

$$G_a[f] \circledast X_a[f] = X_a^*[-f] \circledast X_a[f] = X_a[f] \otimes X_a[f] \tag{4}$$

where $\otimes$ and $\circledast$ are cross-correlation and convolution operator, respectively.

This expression is useful, which means the squared envelope spectrum X_{envs} can be computed from the cross-correlation of X_a with itself, i.e. the correlation of X_a. Thereafter, the convolution and correlation operation on the spectrum of the analytic signal are equivalent, as illustrated in Figure 4. In comparison, the conjugate operation in correlation is more straightforward to understand than the folding operation in convolution. Usually, the correlation is used to represent similarity of a signal to a delayed version of itself. Here, the correlation of X_a can be interpreted as finding the difference frequency components in X_a.

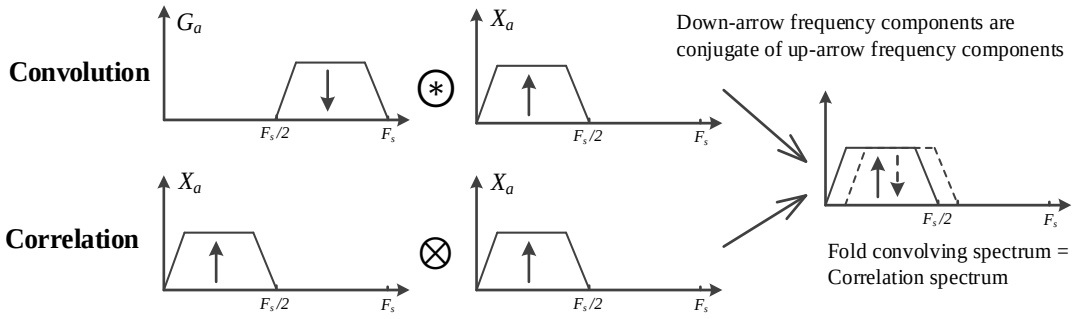

Figure 4 Illustration of convolution and correlation operation of the spectrum of the analytic signal

As usually only a partial band in the spectrum of an analytic signal is selected for correlation, only data within the selected band are involved in the correlation process. Therefore, the correlation of X_a can be updated as:

$$X_a[n] \otimes X_a[n] = \sum_{m=0}^{N} X_a^*[m]X_a[m-n] = \sum_{m=nfL}^{nfH} X_a^*[m]X_a[m-n] \tag{5}$$

where nfL and nfH are the index for low and high cut-off frequencies of the band-pass filter, respectively.

As we know from previous study [11], only a small portion of the squared envelope spectrum is of interest in bearing fault diagnosis, hence there does not need a through computation of correlation. The number of data points effective for squared envelope spectrum calculation are:

$$N_{envs} = 2Nf_{eMax}/F_s \tag{6}$$

where N is the FFT size, f_{eMax} is the interested maximum envelope frequency and F_s is the sampling frequency. In practice, considering the squared envelope is real-valued signal, its spectrum has symmetrical property and thus only half of N_{envs} is required to be calculated, further reducing the computation load.

These indicate spectral correlation can be efficient in terms of computation time. To utilise the scheme proposed in [12] and improve spectrum resolution, the envelope signal can be calculated for cascading from the spectrum of envelope spectrum, as shown in Figure 5. This will be further explored in Section 3.2. Note that only a small number of data points are involved in the IFFT operation, making the calculation of envelope significantly faster than that in Figure 2.

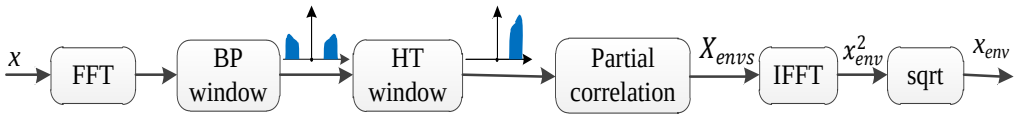

Figure 5 Schematic of spectral correlation based envelope detection

2.3 Band-pass squared rectifier

Since the inner production of an analytic signal with its conjugate is equivalent to the spectral correlation of the analytic signal, one question comes to us: how to understand the inner production of a real-valued signal, i.e. square operation, in the frequency domain?

According to convolution theorem, a square process in the time domain is equivalent to the spectrum being convolved with itself in the frequency domain. For the spectrum $X[n]$ of a real-valued signal x, it has the property of conjugate symmetric [23], i.e. $X[n] = X^*[-n]$, thereby, the convolution of $X[n]$ with itself is equivalent to its correlation:

$$X[n] \circledast X[n] = X[n] \otimes X[n] \tag{7}$$

The convolution of a full baseband signal is presented in Figure 6(a) using an equivalent correlation. It can be seen that aliasing is brought in and the envelope spectrum includes both sum and difference frequency components. Note that, the correlation is actually a circular one due to the circular convolution in Fourier transform and the first aliasing area in Figure 6(a) is caused by this phenomenon. Furthermore, it can be observed that difference frequency components come from the correlation of positive or negative frequency components while sum frequency components are contributed by the cross-correlation between positive and negative ones.

On the occasion when a signal is band-pass filtered, as shown in Figure 6(b), the aliasing problem can be effectively avoided. It has been proved in [14] that through proper zero-padding on both lower

and the upper side of the passband in the frequency domain, the band-pass squared rectifier can achieve the same results as Hilbert transform. In practice, there is no need to transform signals to the frequency domain, zero-pad the spectrum and then perform correlation, as this operation will have the same result apart from there being more computation requirement than frequency domain HT.

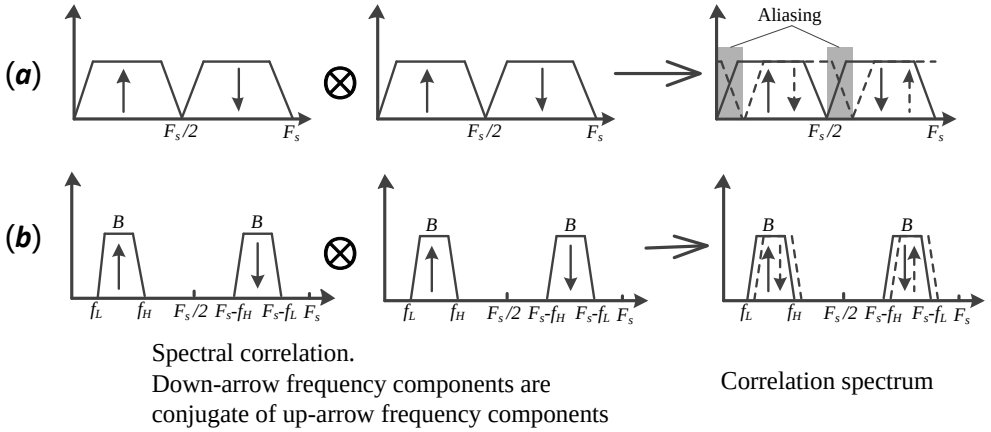

Figure 6 Equivalent spectral correlation of time domain squared operation:
(a) full baseband signal and (b) band-pass filter signal

For a band-pass filtered signal, its square operation in the time domain can avoid the aliasing problem on the condition that its spectrum is already zero-padded, i.e. its lower pass band f_L and upper pass band f_H can satisfy the following criteria:

$$\begin{aligned} f_{\mathrm{L}} &\geq (f_{\mathrm{H}} - f_{\mathrm{L}})/2 \\ F_s/2 - f_H &\geq (f_{\mathrm{H}} - f_{\mathrm{L}})/2 \end{aligned} \tag{8}$$

where F_s is the sampling frequency.

When analysing bearing signal, only low-frequency components in the envelope spectrum are of interest. This indicates aliasing in the high-frequency range of a squared signal is acceptable as they are ineffective for bearing fault diagnosis and can be easily eliminated with a high-pass filter.

Supposing the maximum interested frequency component in the envelope spectrum is f_{eMax}, the band-pass filter restriction in Eq. (8) becomes:

$$\begin{aligned} f_{\mathrm{L}} &\geq f_{eMax}/2 \\ F_s/2 - f_H &\geq f_{eMax}/2 \end{aligned} \tag{9}$$

For a bearing vibration signal sampled at 32 kHz, discussed in this paper, the frequency range of interest for an envelope spectrum is well within 500 Hz (see Section 5.1). According to Eq. (8), a band-pass filter whose pass-band falls inside the range between 250 Hz and 15,750 Hz can effectively avoid aliasing problem within the interested envelope spectrum. Such a requirement can be easily satisfied by the band-pass filters.

2.4 Short-time RMS

Short-time statistical features are another effective method for extracting bearing fault features, which are based on the concept of cyclostationary [24], [25]. The idea of this method is to extract the fault characteristics by finding the cyclic information from the short-time features. The statistical features for calculation can be second and fourth statistical moments, peak value and kurtosis. The short-time statistical feature of signal x by using a statistical operator P, can be written as:

$$ST_x^P(t,d) = P\{x(\tau) \times w_d(\tau - t)\} \tag{10}$$

Where w is the window function, t is the origin of the window, τ is the time variable, and d is the window size. The window function may be different types, such as uniform, triangle, Hanning, or Hamming. After statistical features at all windows are calculated, an FFT operation is performed on the extracted statistical features to find periodic patterns.

For better understanding, the computation process for short-time statistical features is illustrated in Figure 7, where a window of size M slides over the signal x with a step size of S. At each step, a statistical feature P is computed for the signal extracted by the sliding window.

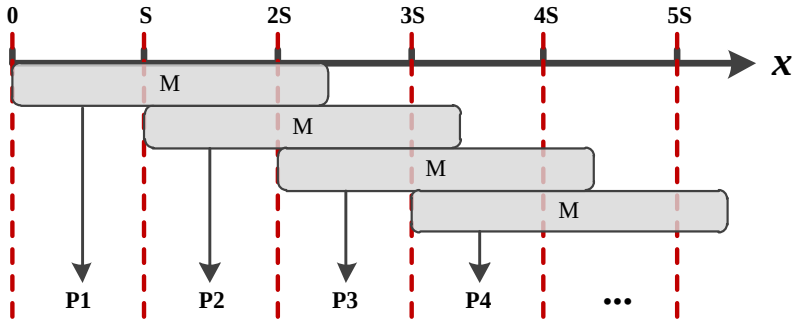

Figure 7 Illustration of short-time statistical feature calculation with step size of S and window size of M

In [24], Behzad et al. showed that the best statistical feature for detecting localised bearing fault is the square root of the second moment, i.e. root mean square (RMS). By considering the definition of RMS in Eq. (11) and the calculation of short-time statistical features in Figure 7, it can be observed that short-time RMS can be regarded as a simplified version of squared rectifier with the low-pass filter and downsample operation being implemented by an overlapped average. The sliding window together with RMS calculation acts like a low-pass filter to omit high-frequency fluctuations in the squared signal and the step size S is the downsample ratio.

$$RMS = \sqrt{\frac{1}{N}\sum_{n=1}^{N} x_n^2} \tag{11}$$

The window length and step size are critical parameters for short-time RMS calculation. The larger the step size, the lower the computation amount. From the view of low-pass filter and down-sampling, the window size M can be determined by the maximum interested frequency f_{eMax} and

sampling frequency F_s and the step size S should be less than half of the window size M to avoid aliasing.

$$M \leq F_s / f_{eMax} \tag{12}$$

$$S \leq M/2 \tag{13}$$

The schematic for a short-time RMS based envelope analysis is presented in Figure 8.

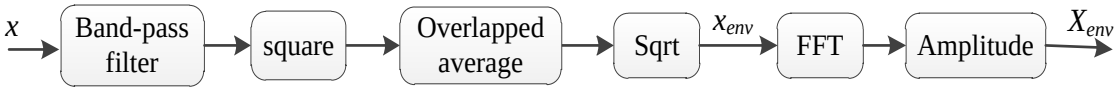

Figure 8 Schematic of short-time RMS based envelope analysis

3 Implementation for high spectrum resolution

From the discussions in Section 2, it shows that the spectral correlation allows the down-sampling process to be performed in the frequency domain and thus provides the potential to speed up the envelop detection in comparison with the frequency domain HT method; the band-pass squared rectifier can effectively avoid aliasing in the interested envelope spectrum with a suitable band-pass filter selected and the short-time RMS can be considered as a simplified version of band-pass squared rectifier, indicating its computation speed should be faster than band-pass squared rectifier. Therefore, the spectral correlation and short-time RMS method are selected for implementation in this section. The scheme proposed in [12] is employed to achieve high envelope spectrum resolution.

Same as the previous implementations [11]–[13], the state-of-the-art Cortex-M4F processor is employed, which has a good balance between signal processing capability and power consumption, making it suitable for wireless sensor nodes that requiring signal processing capabilities. In recent years, this core based processors have been found on the new generation wireless Internet of Things (IOT) solutions, such as the CC3200 WiFi chip from Texas Instruments [26] and nRF52832 BLE solution from Nordic [27]. The algorithms discussed in Section 2 can be confidently migrated into such processors, showing wide suitability of the proposed implementation.

3.1 Overall data processing structure

The overall data processing structure is illustrated in Figure 9. The on-chip analogue to digital converter (ADC), timer and direct memory access (DMA) unit together construct an automatic data acquisition structure to reduce the interrupts to CPU and thus improve the efficiency of signal processing.

In this paper, the sampling frequency is set at 32 kHz and a size of 512 points is processed as a frame. The envelope analysis is mainly computed in the buffer *fBuf,* which is efficiently reused in the calculation procedure. A buffer named *lastFrame* is used to temporarily store data in the last frame so as to achieve the overlap processing and the computed envelope spectrum is stored in the buffer

envOut and then sent to the ZigBee network through UART.

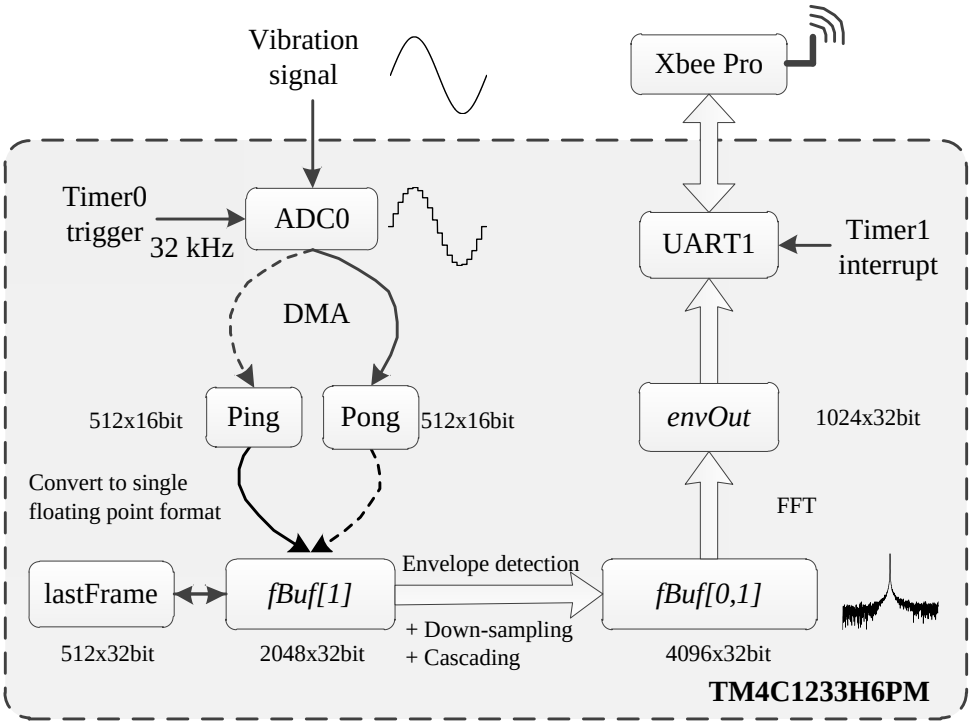

Figure 9 Data flow inside the processor

3.2 Implementation of cascaded spectral correlation

The diagram for cascaded spectral correlation is shown in Figure 10. Similar as the cascaded frequency domain HT in [12], this implementation processes a group of frames with 512 points with an overlap ratio of 50% to minimise edge distortions. For each frame, a 1024-points FFT operation is performed. Considering the maximum interested envelope spectrum frequency is 500Hz, so the number of data points effective for envelope spectrum analysis is 32, according to Eq. (6). Because of the symmetrical property in the spectrum of real-value signal, only half of the data needs to be calculated, i.e. 16 points.

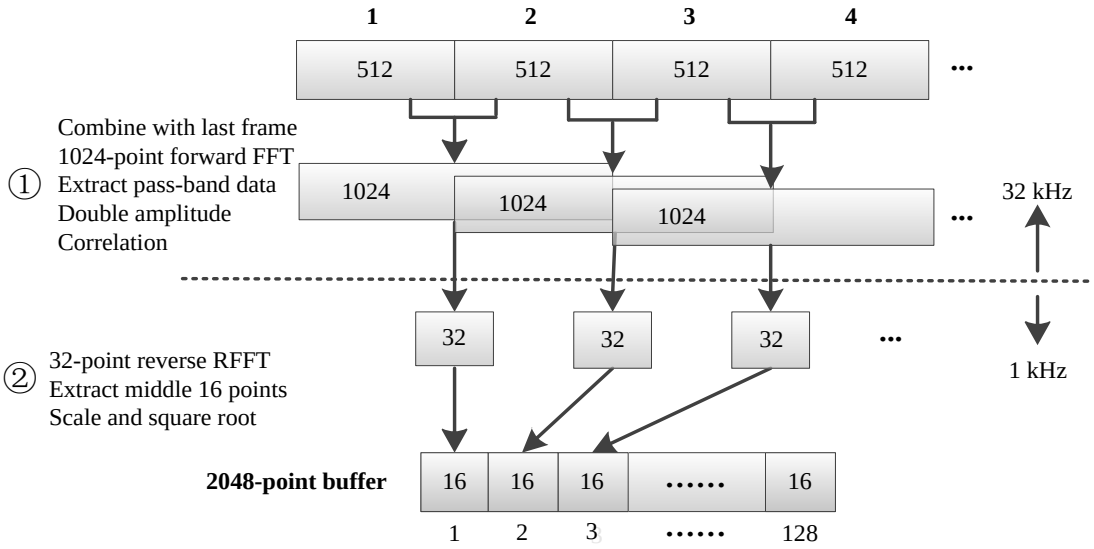

Figure 10 Diagram for cascaded spectral correlation based envelope analysis

In Figure 10, each frame is firstly converted into single floating point format and the first frame is just stored in the buffer *lastFrame. F*rom the second frame, the following operations are performed:

1) Convert data in current frame to single floating point format and combine with data in *lastFrame* buffer to compose a frame with 1024 points.
2) Perform a 1024-points real valued FFT on the composed data frame in the buffer *fBuf[1]*.
3) Extract the frequency components from f_L to f_H and double their amplitude to get the analytic spectrum.
4) Perform a 16-points correlation operation on the obtained analytic spectrum to get the positive part of the squared envelope spectrum. Note that only 16-points correlation instead of 32-points correlation is performed due to the symmetrical property in squared envelope spectrum.
5) Perform a 32-points real-valued IFFT to get the squared envelope signal and a following square root operation to obtain the envelope signal.
6) Extract 16-points in the middle of the calculated envelope signal and append them in the buffer *fBuf[0]*.

After 128 frames of data are calculated, the buffer *fBuf[0]* are filled with 2048 points of envelope signal and finally a 2048-points real valued forward FFT is performed to get the envelope spectrum. This finishes one cycle of envelope analysis.

To verify the implementation of spectral correlation and the consecutiveness of the cascaded envelope, a simulated modulating signal is processed on the processor and the detected envelope from first three frames are extracted and illustrated in Figure 11. It can be observed that the obtained envelope has a good match with the upper outline of the modulating signal in Figure 11(d). Note that small mismatches can be seen on the edges of the obtained envelope in Figure 11 (b) and (c), which are not included for cascaded processing.

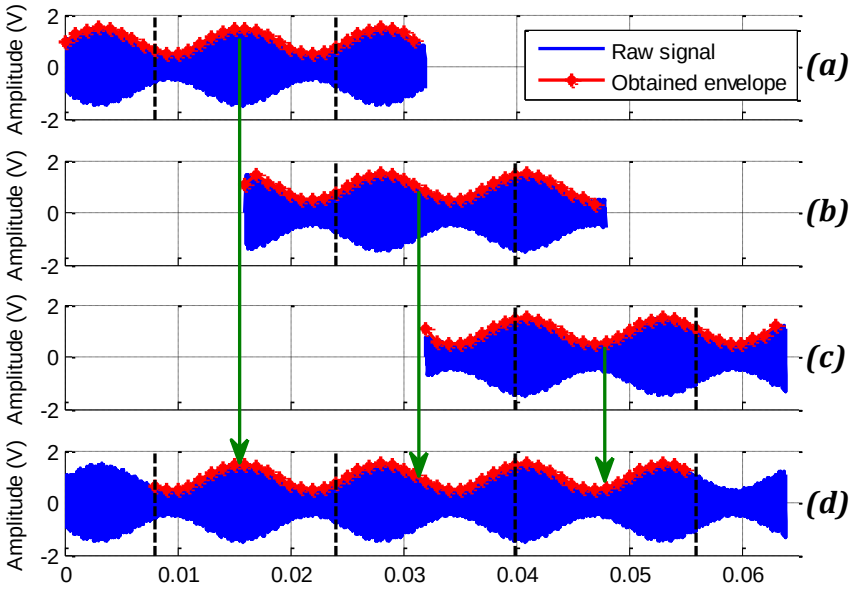

Figure 11 Illustration of cascaded spectral correlation for envelope calculation:
(a) first frame result, (b) second frame result, (c) third frame result and (d) cascaded envelope

3.3 Implementation of cascaded short-time RMS

The diagram for cascaded short-time RMS is presented in Figure 12, which also follows the overall data processing structure in Figure 12 but with slight changes in the cascading part. The collected data are also processed frame by frame with the size of 512 points. Considering the maximum interested envelope spectrum frequency is 500Hz, the window size is set as 64 and step size is set as 32, according to Eq. (12) and (13).

In Figure 12, each frame is firstly filtered by an 81-tap FIR type band-pass filter. Then, the short-time RMS of the filtered data is computed and stored in a buffer. Note that for the first frame of data, 13 effective feature data are produced due to the first 40 data of the FIR filter being invalid and thus the short RMS calculation actually starts from the third step.

From the second frame until the second last frame, last 32 points from the previous frame are concatenated in front of the current frame of data for the short-time RMS calculation and hence they produce 16 points of effective feature data. For the last frame, only 3 points of feature data are required for filling the 2048-point buffer. After the 2048-point buffer is full, the spectrum of short-time RMS features is computed by FFT calculations to get the envelope spectrum.

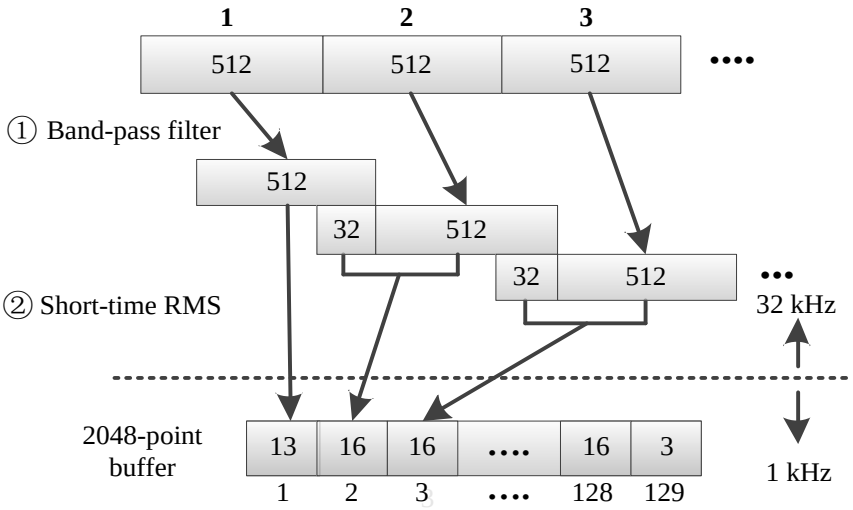

Figure 12 Diagram for cascaded short-time RMS based envelope analysis

To verify the implementation of cascaded short-time RMS, a simulated modulating signal is processed on the processor and the calculated results are illustrated in Figure 13. It shows the calculated short-time RMS follows the trend of the outline of the modulating signal but with its amplitude proportionally attenuated, which can be explained by the squared operation in short-time RMS. This means short-time RMS has similar frequency components as the envelope of the signal and thus can also be used for bearing fault diagnosis.

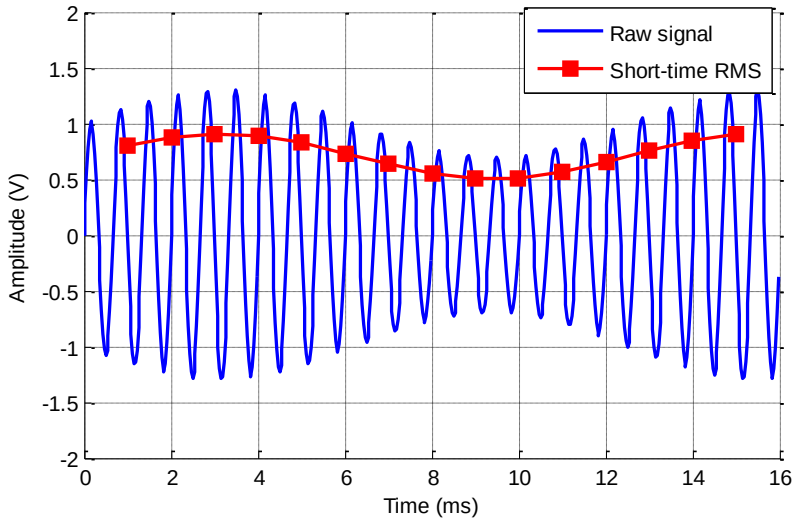

Figure 13 Illustration of short-time RMS calculation on a simulated modulating signal.

3.4 Computation speed benchmark

In the above implementations, the envelope detection part requires real-time calculations. For both implementations in the cascaded spectral correlation and cascaded short-time RMS, the data is processed with a frame size of 512 points. With the sampling frequency at 32 kHz, the deadline for calculating one frame is 512/32 = 16 ms.

Several methods can be employed to measure the computation time for one part of codes, for example, setting break points in the beginning and end of the codes and count CPU clocks using tools integrated in the development environment, or changing a GPIO output in the codes and then measuring the outputs using oscilloscope. If the program is written on the real-time operating system (RTOS), namely TI-RTOS [30], the timestamp function can be a convenient method. In this paper, the timestamp method is employed.

The time for processing one frame of data by the frequency domain HT method [13] and the implemented two methods are measured and presented in Figure 14. It can be seen that both spectral correlation and short-time RMS show faster computation speed than the previously implemented frequency domain HT method does. Note that the computation speed of spectral correlation is affected by the data points involved with spectral correlation, i.e. data length from nfH to nfL in Eq. (5), and data points useful for squared envelope spectrum analysis N_{envs} in Eq. (6). This means the pass band width, FFT size and sampling frequency have an influence on the computation time of spectral correlation. For this implementation, the sampling frequency and FFT size have been fixed, so the pass band width becomes the main influence factor. As shown in Figure 14, the computation time of spectral correlation increases linearly with the pass band width. In practice, the optimum band-pass filter usually has a narrow bandwidth, typically less than 3 kHz for bearing signals analysed in this paper, meaning the computation time is typically less than 4.2 ms. This is more than two times faster than the frequency domain HT method in [13].

For short-time RMS, the computation time for one frame is measured as about 2.2 ms when an 81-tap FIR band-pass filter is employed, which is more than five times faster than the frequency domain HT method in [13]. This time consumption is even lower than the smallest one (3.12 ms) in the spectral correlation based method, meaning short-time RMS method is more computation efficient than spectral correlation one.

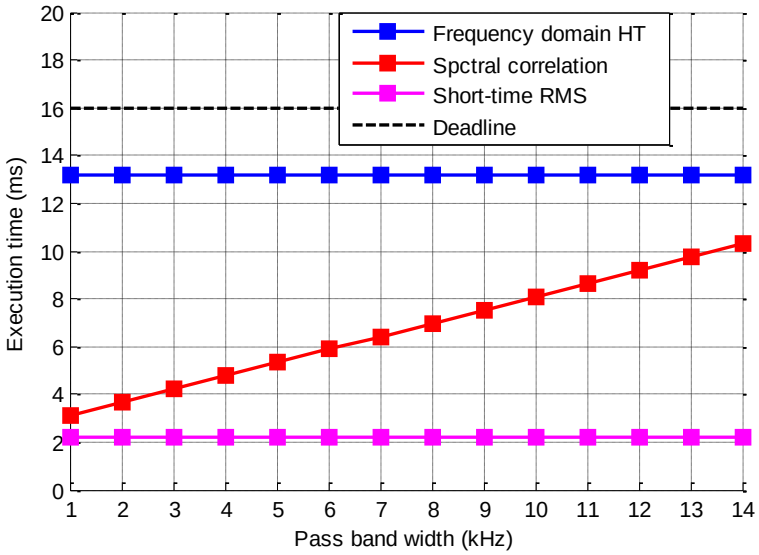

Figure 14 Computation time comparison for one frame data

4 Simulation study

To validate the performance of implemented algorithms for extracting bearing fault features, a group of rolling bearing signals are simulated according to Eq. (14) [28], [29].

$$\begin{aligned} x(t) &= s(t) + n(t) = \sum_i A_0 h(t - iT) + n(t) \\ h(t) &= \exp(-Ct)\cos(2\pi f_n t) \\ n(t) &= MA_0 rand() \end{aligned} \tag{14}$$

where A_0 is the amplitude of the impact force; T is the average period of impulse series which equals 1/83s≈0.012s; f_n is the structural resonance frequency which equals 4500Hz; C is the damping coefficient which equals 900; $rand()$ is a random value generator function and can generate a random value in the range of (-1,1); M controls the severity of the added noise.

The simulated bearing signals and their spectrum are presented in Figure 15, with different noise severity levels. In Figure 15(a), a series of impulses can be clearly in the time domain signal and high spectrum appears around 4500 Hz, which is in accordance with the resonance frequency. As the noise level increases from Figure 15(a) to (d), the impulses are gradually submerged by noises. Note that these signals are directly generated on the processor because the processor doesn't have sufficient memory to store the simulated signals.

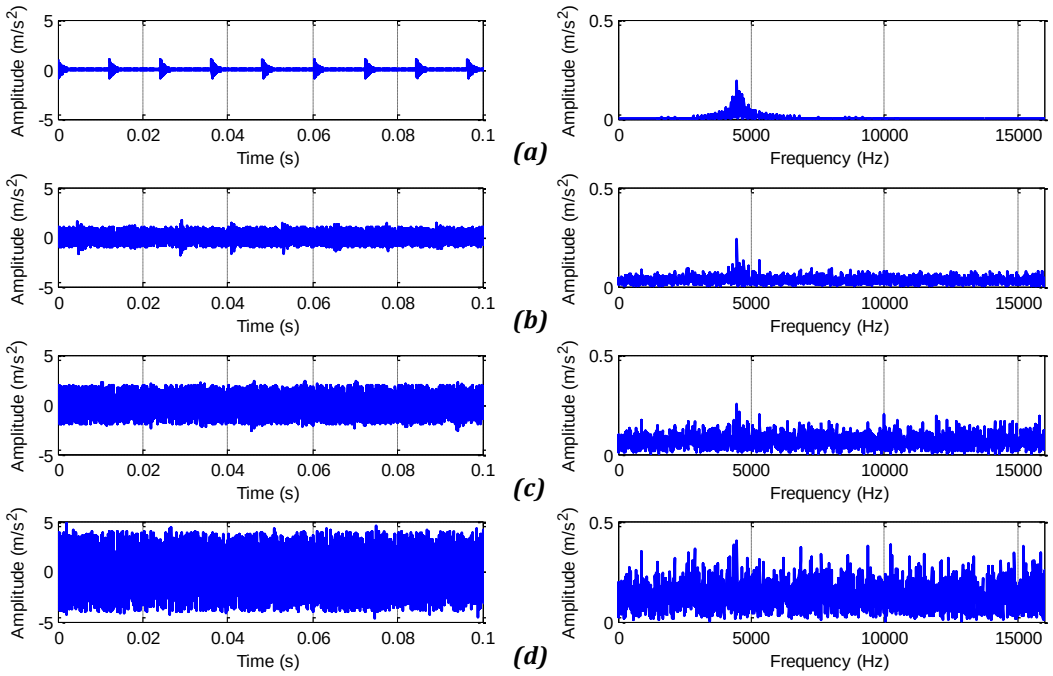

Figure 15 Simulated bearing signal in the time domain and frequency domain with different noise levels: (a) no noise, (b) noise level of A_0, (c) noise level of $2A_0$ and (d) noise level of $4A_0$

Then, these signals are processed by the frequency domain HT (FHT) and the two methods implemented in Section 3, i.e. spectral correlation (SCORR) and short-time RMS (STRMS). The

processing results are presented in Figure 16. It can be observed that the harmonics of the fault frequency can be clearly observed for all three methods when the noise level is less than two times of the impulse amplitude and the fault frequencies are not so clear when the noise level increases to four times of the impulse amplitude. Specially, the higher order harmonics in STRMS method is more attenuated in comparison with those in FHT and SCORR methods. This is in accordance with the high attenuation effect of the overlapped average process in STRMS method. In addition, the processing results of FHT and SCORR show high similarity, which means the implemented SCORR and STRMS methods have achieved similar level of accuracy.

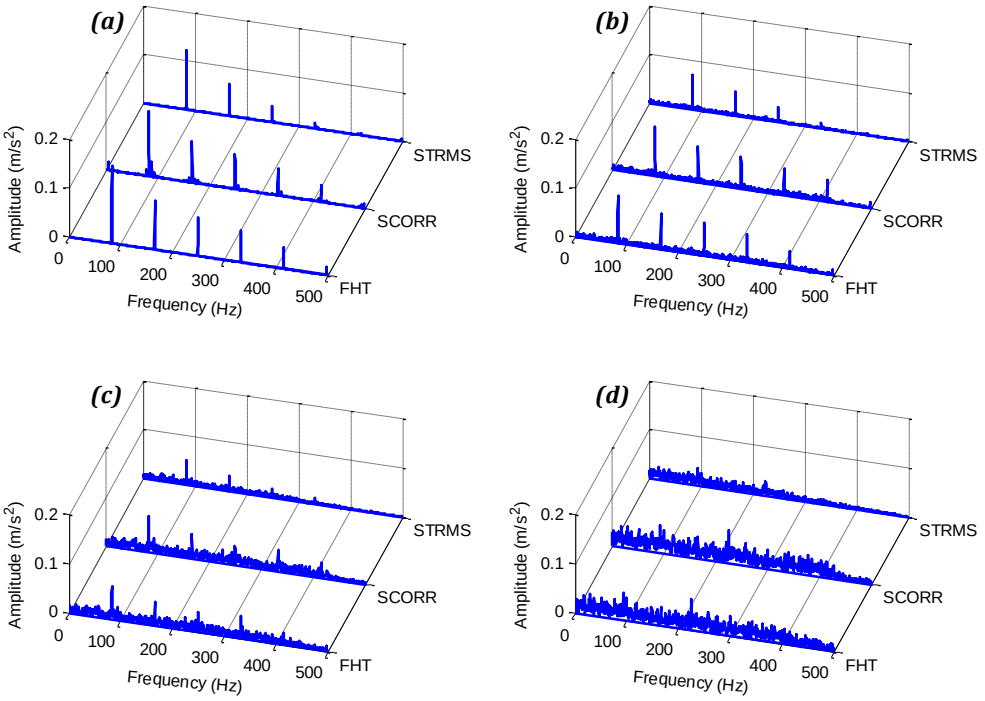

Figure 16 Comparsion of processing results by different methods for bearing signals with different noise levels: (a) no noise, (b) noise level of A_0, (c) noise level of $2A_0$ and (d) noise level of $4A_0$

5 Experimental results

5.1 Bearing test rig description

To evaluate the effectiveness of the implemented envelope analysis methods, they are employed to analyse true bearing fault signals. The bearing test rig is shown in Figure 17(a), which is composed of five main parts: an electrical induction motor, shaft couplings, a DC generator, bearings and motion shaft. The bearing in the test rig is N406 cylindrical roller type. During the test, the shaft ran at a full speed of 1460 rpm, i.e. 24.3 Hz.

Four bearing conditions are simulated on the test rig, as shown in Figure 17(b-e). The healthy bearing was employed for producing the baseline signal and the other three bearings were seeded with outer race fault, inner race fault and roller fault. A piezoelectric (PE) type accelerometer was mounted on the bearing house horizontally to collect the vibration signal. The accelerometer was

connected to the assembled wireless sensor node based on TM4C123GH6PM for data processing and wireless transmission, as shown in Figure 17(f).

The localised fault frequencies are calculated and listed in Table 1. It can observed that the inner race fault has the highest characteristic frequency, at 135.5 Hz, whose 3rd harmonic frequency (406.5 Hz) is within 500 Hz. This means fault frequencies of interests are all within 500 Hz, which is used for determining key parameters in Eq. (6) for spectral correlation and Eq. (12) for short-time RMS.

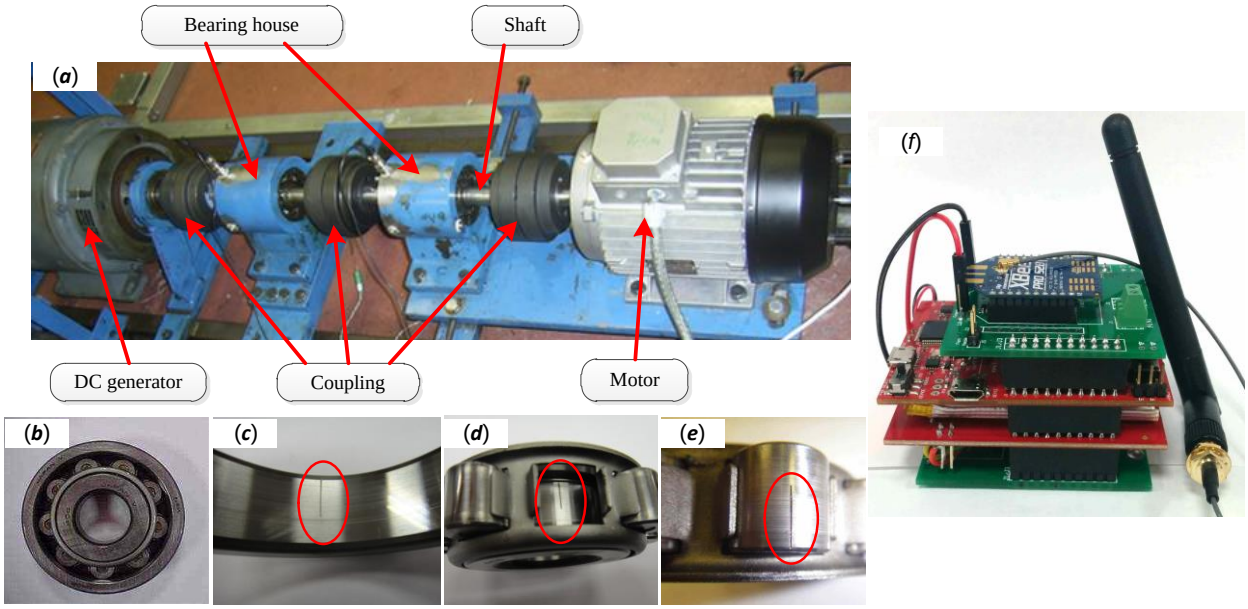

Figure 17 Bearing test rig and bearings for experiments: (a) bearing test rig, (b) healthy bearing, (c) bearing with outer race defect, (d) bearing with inner race defect, (e) bearing with roller defect and (f) wireless sensor node

Table 1 Bearing fault characteristic frequencies

Defect location	Fault frequency (Hz)
Inner race (BPFI)	**135.5**
Outer race (BPFO)	**83.5**
Ball (BSF)	**48.4**

5.2 Results and discussion

The vibration signals collected from the three bearing fault conditions are analysed by the two methods implemented in Section 3, together with the frequency domain HT method implemented in [13]. The sampling frequency is set as 32 kHz, same as the implementation in Section 3. The fast kurtogram method implemented in [13] is employed to select the optimal band-pass filters. A diagram for implementing fast kurtogram in the wireless CM system is illustrated in Figure 18, in which the system works in two modes, namely configuration mode and monitoring mode. The configuration mode is used for updating the optimal band-pass filter coefficients and it operates at the installation time of the system and during a period when a significant change appears in the monitoring mode or at a given long time interval. Most of the time, the system works in the monitoring mode, in which the wireless sensor node uses the optimum band-pass filter calculated in

the configuration mode to analyse the vibration signal and transmit the envelope spectrum to the host computer for fault diagnosis. The calculated optimum band-pass filters by fast kurtogram are: 8-10.67 kHz for outer race fault signal, 2.67-5.33 kHz for inner race fault signal and 4-5 kHz for roller fault signal.

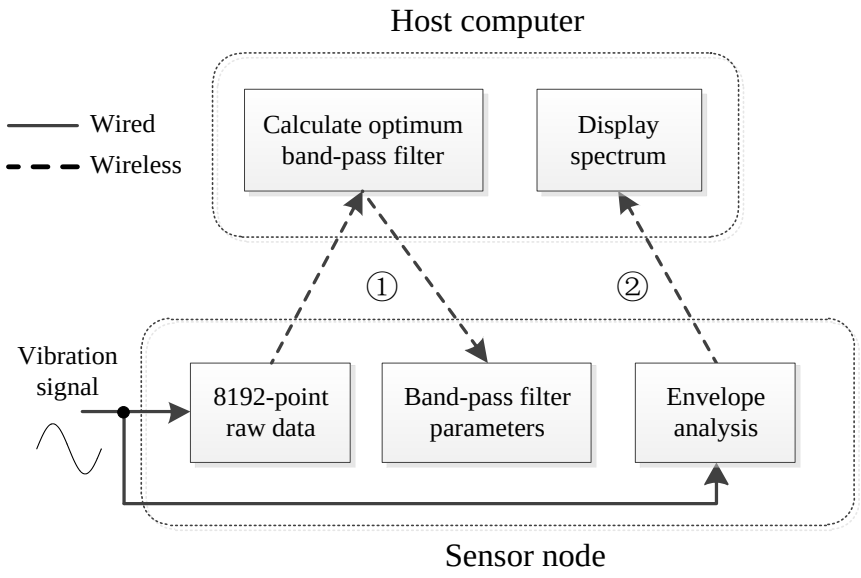

Figure 18 Diagram for implementing fast kurtogram to select optimum band-pass filter

The analysis results for outer race fault, inner race fault and roller fault are presented in Figure 19, Figure 20 and Figure 21, respectively. Take the processing results for outer race for example. The harmonics of the outer race fault characteristic frequency can be clearly observed in the envelope spectrum of all three algorithms, as shown in Figure 19(b), (c) and (d), verifying the existence of the outer race fault on the bearing component. In comparison, the higher harmonics from short-time RMS method in Figure 19(d) are smaller than those from frequency domain HT in Figure 19(b) and spectral correlation in Figure 19(c). This can be explained by the high attenuation effect of the overlapped average process in short-time RMS based method. For frequency domain HT and spectral correlation, they can reveal the same amount of harmonics and the amplitudes of the corresponding harmonic components are similar. However, more noises can be observed in the low-frequency range of spectral correlation than those in frequency domain HT. Nevertheless, these differences cause little influences on the diagnostic results.

Similar processing results can be observed for the inner race fault and roller fault in Figure 19 and Figure 20, respectively. Note that the third harmonic for inner race fault in Figure 19(d) and fourth harmonic for roller fault in Figure 20(d) can be hardly seen in the results from short-time RMS method.

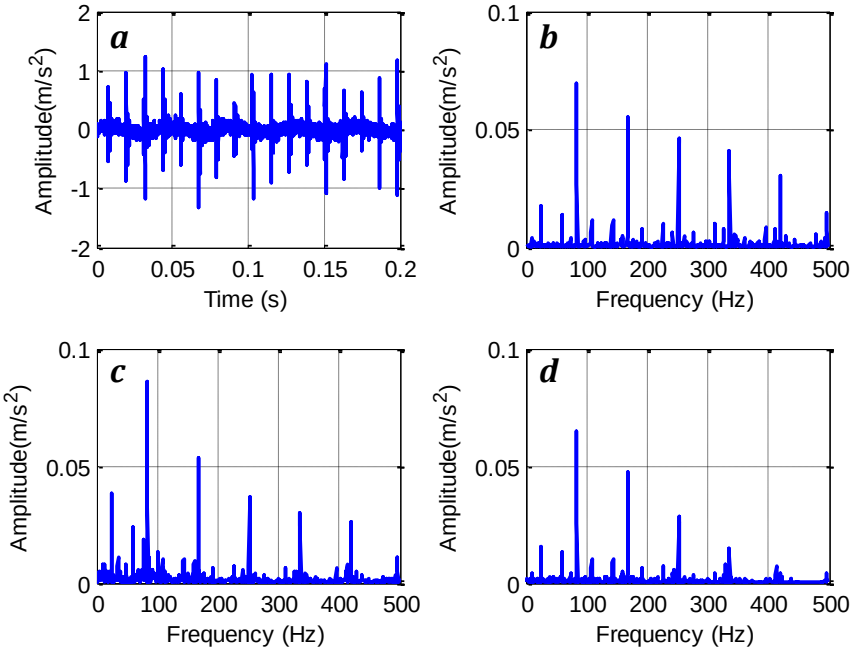

Figure 19 Detection results for a bearing vibration signal with outer race fault: (a) raw signal, (b) envelope spectrum from frequency domain HT, (c) envelope spectrum from spectral correlation and (d) envelope spectrum from short-time RMS

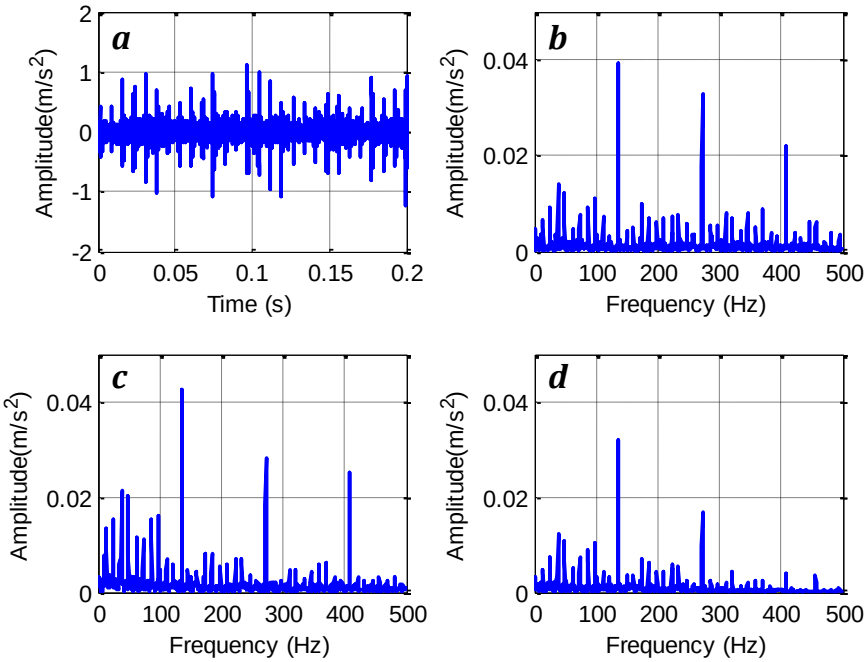

Figure 20 Detection results for a bearing vibration signal with inner race fault: (a) raw signal, (b) envelope spectrum from frequency domain HT, (c) envelope spectrum from spectral correlation and (d) envelope spectrum from short-time RMS

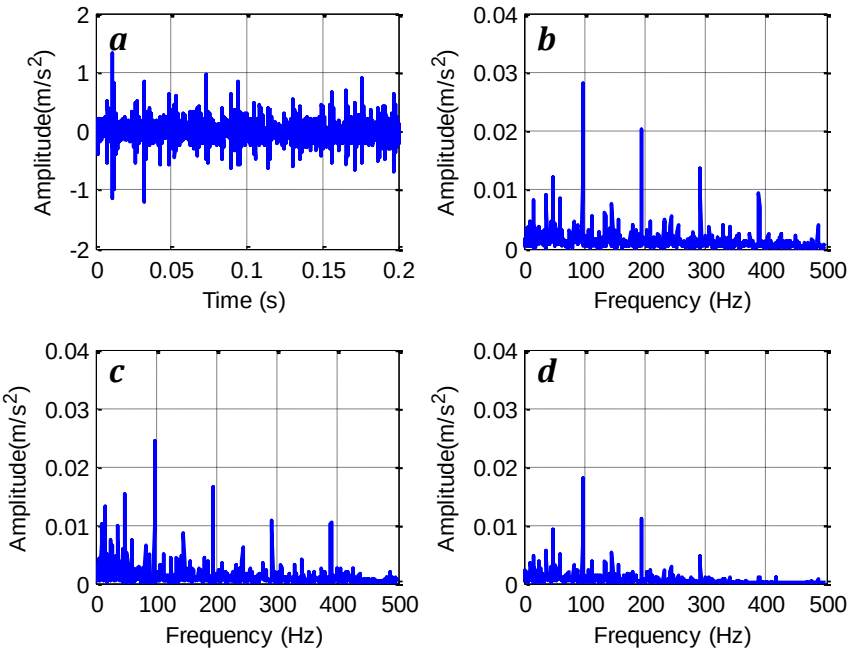

Figure 21 Detection results for a bearing vibration signal with roller fault: (a) raw signal, (b) envelope spectrum from frequency domain HT, (c) envelope spectrum from spectral correlation and (d) envelope spectrum from short-time RMS

5.3 Data throughput analysis

All these three methods produce an envelope spectrum with 1024 points, so their transmission data size is exactly the same. This data has been converted to 16-bit resolution for transmission over the wireless network. This 1024 points envelope spectrum is calculated from about 129 frames of the raw data set, each of which has 512 points of data. This means the resultant data set is only about 1024/512/129≈0.0155, i.e. 1.55%, of the raw data set, which is a very high reduction ratio.

As the band-pass filter parameters can be adaptively updated, there also requires a configuration packet. The HT frequency domain and spectral correlation method only require the two boundaries of the band-pass filter while the short-time RMS method requires the coefficients of the FIR filter, that is 81 points of floating type data in this implementation. From this point of view, the spectral correlation method is better than the short-time RMS method in terms of fast parameter configuration.

6 Conclusion

In this paper, the envelope analysis method is studied to explore its efficient implementations in a wireless sensor node for condition monitoring. It shows that the spectral correlation allows the down-sampling process to be performed in the frequency domain and thus provides the potential to speed up the computation; the short-time RMS method can be considered as a simplified squared rectifier and it can avoid aliasing in the interested frequency band of the envelope spectrum with a proper band-pass filter selected. On this basis, the spectral correlation and short-time RMS methods are

implemented on the resource limited wireless sensor nodes, showing satisfactory computation speed improvement and good capability for identifying localized bearing faults. These two implemented methods make the envelope analysis even more suitable for being embedded on resource limited wireless sensor nodes for bearing fault diagnosis. Overall, the benefits of the proposed implementation include:

- Result data set is much smaller than raw data set, allowing data transmission over the bandwidth limited wireless sensor network
- Computation speed is fast, allowing lower power consumption of the wireless sensor nodes
- Memory usage is efficient, allowing the implementation on low cost wireless sensor nodes
- Envelope spectrum resolution is high, allowing reliable fault diagnosis

References

[1] L. Hou and N. W. Bergmann, "Novel Industrial Wireless Sensor Networks for Machine Condition Monitoring and Fault Diagnosis," *IEEE Trans. Instrum. Meas.*, vol. 61, no. 10, pp. 2787–2798, Oct. 2012.

[2] B. Lu and V. C. Gungor, "Online and Remote Motor Energy Monitoring and Fault Diagnostics Using Wireless Sensor Networks," *IEEE Trans. Ind. Electron.*, vol. 56, no. 11, pp. 4651–4659, Nov. 2009.

[3] A. Prijic, L. Vracar, D. Vuckovic, D. Milic, and Z. Prijic, "Thermal Energy Harvesting Wireless Sensor Node in Aluminum Core PCB Technology," *IEEE Sens. J.*, vol. 15, no. 1, pp. 337–345, Jan. 2015.

[4] J. H. Jang, D. F. Berdy, J. Lee, D. Peroulis, and B. Jung, "A Wireless Condition Monitoring System Powered by a Sub-100 W Vibration Energy Harvester," *IEEE Trans. Circuits Syst. Regul. Pap.*, vol. 60, no. 4, pp. 1082–1093, 2013.

[5] J. Davidson and C. Mo, "Recent Advances in Energy Harvesting Technologies for Structural Health Monitoring Applications," *Smart Mater. Res.*, vol. 2014, p. e410316, Apr. 2014.

[6] T. R. Burchfield, S. Venkatesan, and D. Weiner, "Maximizing throughput in zigbee wireless networks through analysis, simulations and implementations," in *Proc. Int. Workshop Localized Algor. Protocols WSNs*, 2007, pp. 15–29.

[7] N. Tandon and A. Choudhury, "A review of vibration and acoustic measurement methods for the detection of defects in rolling element bearings," *Tribol. Int.*, vol. 32, no. 8, pp. 469–480, Aug. 1999.

[8] V. C. Gungor and G. P. Hancke, "Industrial Wireless Sensor Networks: Challenges, Design Principles, and Technical Approaches," *IEEE Trans. Ind. Electron.*, vol. 56, no. 10, pp. 4258–4265, Oct. 2009.

[9] T. Sreenuch, A. Tsourdos, and I. K. Jennions, "Distributed embedded condition monitoring systems based on OSA-CBM standard," *Comput. Stand. Interfaces*, vol. 35, no. 2, pp. 238–246, 2013.

[10] Y. Kaicheng and Z. Chaosheng, "Vibration data fusion algorithm of auxiliaries in power plants based on wireless sensor networks," in *2011 International Conference on Computer Science and Service System (CSSS)*, 2011, pp. 935–938.

[11] G.-J. Feng, J. Gu, D. Zhen, M. Aliwan, F.-S. Gu, and A. D. Ball, "Implementation of envelope analysis on a wireless condition monitoring system for bearing fault diagnosis," *Int. J. Autom. Comput.*, vol. 12, no. 1, pp. 14–24, Feb. 2015.

[12] G. Feng, D. Zhen, X. Tian, F. Gu, and A. D. Ball, "A Novel Method to Improve the Resolution of Envelope Spectrum for Bearing Fault Diagnosis Based on a Wireless Sensor Node," in *Vibration Engineering and Technology of Machinery*, J. K. Sinha, Ed. Springer International Publishing, 2015, pp. 765–775.

[13] G. Feng, X. Tian, J. X. Gu, D. Yang, F. Gu, and A. Ball, "An adaptive envelope analysis in a wireless sensor network for bearing fault diagnosis using fast kurtogram algorithm," presented at the Comadem 2014, Brisbane, Australia, 2014.

[14] D. Ho and R. B. Randall, "Optimisation Of Bearing Diagnostic Techniques Using Simulated And Actual Bearing Fault Signals," *Mech. Syst. Signal Process.*, vol. 14, no. 5, pp. 763–788, Sep. 2000.

[15] S. A. McInerny and Y. Dai, “Basic vibration signal processing for bearing fault detection,” *IEEE Trans. Educ.*, vol. 46, no. 1, pp. 149–156, 2003.
[16] H. Konstantin-Hansen, “Envelope analysis for diagnostics of local faults in rolling element bearings,” *Brüel Kja Er Den.*, 2003.
[17] H. Li, X. Zhang, and F. Xu, “Experimental Investigation on Centrifugal Compressor Blade Crack Classification Using the Squared Envelope Spectrum,” *Sensors*, vol. 13, no. 9, pp. 12548–12563, Sep. 2013.
[18] M. Ahmed, F. Gu, and A. D. Ball, “Fault Detection of Reciprocating Compressors using a Model from Principles Component Analysis of Vibrations,” *J. Phys. Conf. Ser.*, vol. 364, no. 1, p. 12133, May 2012.
[19] K. Jiang, G. Xu, L. Liang, T. Tao, and F. Gu, “The Recovery of Weak Impulsive Signals Based on Stochastic Resonance and Moving Least Squares Fitting,” *Sensors*, vol. 14, no. 8, pp. 13692–13707, Jul. 2014.
[20] R. B. Randall and J. Antoni, “Rolling element bearing diagnostics—A tutorial,” *Mech. Syst. Signal Process.*, vol. 25, no. 2, pp. 485–520, Feb. 2011.
[21] I. Howard, “A Review of Rolling Element Bearing Vibration’Detection, Diagnosis and Prognosis’,” DTIC Document, 1994.
[22] M. Feldman, “Hilbert transform in vibration analysis,” *Mech. Syst. Signal Process.*, vol. 25, no. 3, pp. 735–802, Apr. 2011.
[23] R. G. Lyons, *Understanding Digital Signal Processing*, 3 edition. Upper Saddle River, NJ: Prentice Hall, 2010.
[24] M. Behzad, A. R. Bastami, and D. Mba, “Rolling bearing fault detection by short-time statistical features,” *Proc. Inst. Mech. Eng. Part E J. Process Mech. Eng.*, vol. 226, no. 3, pp. 229–237, Aug. 2012.
[25] A. C. McCormick and A. K. Nandi, “Cyclostationarity in rotating machine vibrations,” *Mech. Syst. Signal Process.*, vol. 12, no. 2, pp. 225–242, 1998.
[26] Texas Instruments, CC3200 Datasheet, Available from: <http://www.ti.com/lit/ds/symlink/cc3200.pdf> Feb-2015.
[27] Nordic semiconductor, nRF52382 Datasheet, Available from: < http://infocenter.nordicsemi.com/pdf/nRF52832_PS_v1.3.pdf>, 17-Feb-2016.
[28] R. B. Randall, J. Antoni, and S. CHOBSAARD, “The Relationship between spectral correlation and envelope analysis in the diagnostics of bearing faults and other cyclostationary machine signals,” *Mech. Syst. Signal Process.*, vol. 15, no. 5, pp. 945–962, Sep. 2001.
[29] X. Chen, F. Feng, and B. Zhang, “Weak Fault Feature Extraction of Rolling Bearings Based on an Improved Kurtogram,” *Sensors*, vol. 16, no. 9, p. 1482, Sep. 2016.
[30] Texas Instruments, TI-RTOS: A real-time operating system for TI devices, Available from: <http://www.ti.com/lit/ml/sprt646a/sprt646a.pdf>, 2015.